

# Mixing-layer-height-referenced ozone vertical distribution in the lower troposphere of Chinese megacities: Stratification, classification, meteorological, and photochemical mechanisms

Zhiheng Liao<sup>a, b</sup>, Meng Gao<sup>c</sup>, Jinqiang Zhang<sup>d, e</sup>, Jiaren Sun<sup>f</sup>, Jiannong Quan<sup>a</sup>, Xingcan Jia<sup>a</sup>, Yubing Pan<sup>a</sup>, Shaojia Fan<sup>b, g</sup>

5

<sup>a</sup> Institute of Urban Meteorology, Chinese Meteorological Administration, Beijing, China

<sup>b</sup> School of Atmospheric Sciences, Sun Yat-Sen University, Zhuhai, China

<sup>c</sup> Department of Geography, Hong Kong Baptist University, Hong Kong SAR, China

<sup>d</sup> Key Laboratory of Middle Atmosphere and Global Environment Observation, Institute of Atmospheric Physics, Chinese Academy of Sciences, Beijing, China

10

<sup>e</sup> College of Earth and Planetary Sciences, University of Chinese Academy of Sciences, Beijing 100049, China

<sup>f</sup> Key Laboratory of Urban Ecological Environmental Simulation and Protection of Ministry of Environmental Protection, South China Institute of Environmental Sciences, Ministry of Ecology and Environment of the PRC, Guangzhou, China

15

<sup>g</sup> Guangdong Provincial Observation and Research Station for Climate Environment and Air Quality Change in the Pearl River Estuary, Key Laboratory of Tropical Atmosphere–Ocean System, Ministry of Education, Southern Marine Science and Engineering Guangdong Laboratory (Zhuhai), Zhuhai, China

**Corresponding author:** S. J. Fan (eesfsj@mail.sysu.edu.cn)

20

**Abstract:** Traditional tropospheric ozone ( $O_3$ ) climatology uses a simple average substantially smoothed stratification structure in individual  $O_3$  profiles, limiting our ability to properly describe and understand how  $O_3$  is vertically distributed at the interface between the mixing layer (ML) and free troposphere (FT). In this study, we collected 1,897 ozonesonde profiles from two Chinese megacities (Beijing and Hong Kong) over the period 2000–2022 to investigate climatological vertical heterogeneity of lower-tropospheric  $O_3$  distribution with a mixing-layer-height-referenced ( $h$ -referenced) vertical coordinate system. The mixing layer height ( $h$ ) was first estimated following an integral method that integrates the information of temperature, humidity, and cloud. After that, a so-called  $h$ -referenced vertical distribution of  $O_3$  was determined by averaging all individual profiles expressed as a function of  $z/h$  rather than  $z$  (where  $z$  is altitude). We found that the vertical stratification of  $O_3$  is distributed heterogeneously in the lower troposphere, with stronger vertical gradients at the surface layer and ML–FT interface.

25

There are low vertical autocorrelations of  $O_3$  between the ML and FT, but high autocorrelations within each of the two atmospheric compartments. These results suggest that the ML–FT interface acts as a geophysical “barrier” separating air masses of distinct  $O_3$  loadings. This barrier effect varies with season and city, with an ML-to-FT detrainment barrier in summer (autumn) and an FT-to-ML entrainment barrier in other seasons in Beijing (Hong Kong). Based on Student’s  $t$  test, daily  $h$ -referenced  $O_3$  profiles were further classified into three typical patterns:

30

35  $MLO_3$ -dominated,  $FTO_3$ -dominated, and uniform distribution. Although the  $FTO_3$ -dominated pattern occurs most frequently during the whole study period (69% and 54% of days in Beijing and Hong Kong, respectively), the  $MLO_3$ -dominated pattern prevails in the photochemical active season, accounting for 47% of summer days in Beijing and 54% of autumn days in Hong Kong. These occurrences of the  $MLO_3$ -dominated pattern are significantly more frequent than in previously reported results at northern mid-latitudes, indicating intensive photochemical  $MLO_3$  production under the high-emission background of Chinese megacity. From  $FTO_3$ -dominated to  $MLO_3$ -dominated pattern, the  $O_3$  precursor  $CH_2O$  ( $NO_2$ ) experiences a substantial increase (decrease) in Beijing,

but a slight change in Hong Kong. Vertically, the increment of  $\text{CH}_2\text{O}$  is larger in the upper ML and the decrement of  $\text{NO}_2$  is larger in the lower ML. Such vertical changes in  $\text{O}_3$  precursors push  $\text{O}_3$  production sensitivity away from the VOC-limited regime and facilitate high-efficiency production of  $\text{O}_3$  via photochemical reactions, particularly in the upper ML of Beijing.

## 1 Introduction

Ozone ( $\text{O}_3$ ), the dominant precursor of hydroxyl radicals, plays a crucial role in tropospheric chemistry. It is also an important greenhouse gas closely related to climate change and environmental issues (Seinfeld and Pandis, 2016;Monks et al., 2015). Being an air pollutant,  $\text{O}_3$  can influence air quality on a hemispheric scale, exerting detrimental effects on human health and vegetation (Fleming et al., 2018;Mills et al., 2018). Tropospheric  $\text{O}_3$  is primarily formed through a complex series of photochemical reactions between nitrogen oxides (NOx) and volatile organic compounds (VOCs) in the presence of sunlight (Seinfeld and Pandis, 2016). There are substantial emissions of NOx and VOCs in urban regions, where most of the population and industry are concentrated. As a result, elevated  $\text{O}_3$  concentrations in the lower troposphere remain a persistent environmental problem in urban regions around the world (Lu et al., 2018). Significant efforts have been made to understand  $\text{O}_3$  pollution in different cities (Monks et al., 2015). However, most previous studies were based on ground-based observations, and gave only limited insight into  $\text{O}_3$  vertical distribution.

$\text{O}_3$  vertical distribution in the lower troposphere can provide very important information for mechanistic understanding of surface  $\text{O}_3$  pollution (He et al., 2021;Lin et al., 2010;Jaffe, 2011;Yates et al., 2017). One of the major advantages when dealing with  $\text{O}_3$  profile data is able to discriminate the two specific  $\text{O}_3$  components corresponding to the two “reservoirs”—the mixing layer (ML) and the free troposphere (FT)—and therefore, to determine the direction and intension of vertical exchange processes across the ML-FT interface. Several studies have been made trying to resolve the  $\text{O}_3$  vertical exchange problem in the lower troposphere (Neuman et al., 2012;Berkes et al., 2016;Kaser et al., 2017;Trousdale et al., 2016;Zhao et al., 2019;Lin et al., 2010;Zhu et al., 2020). For example, based on tethered ozone soundings during a four-day ozone episode in southern Taiwan, Lin et al. (2010) revealed that the increase rate of surface  $\text{O}_3$  concentration due to the downward mixing of the  $\text{O}_3$  from the  $\text{O}_3$  reservoir layers can be as high as 12–24 ppbv  $\text{h}^{-1}$  in the late morning. Based on 214 aircraft vertical profiles in Colorado during summer 2014, Kaser et al. (2017) investigated the  $\text{O}_3$  vertical gradient between the ML and the FT in order to estimate the FT-to-ML  $\text{O}_3$  entrainment and to evaluate its representation in the WRF-Chem model. Their study focusing on the  $\text{O}_3$  entrainment highlighted deficiencies in the model, indicating an overestimation of the  $\text{O}_3$  entrainment and a too-efficient vertical mixing in the lower ML. These deficiencies were found to originate mainly from errors in the entrainment rate and ML height during the morning and an erroneous representation of the  $\text{O}_3$  gradient at the ML-FT interface during the rest of the day. Overall, by measuring the specific terms in the vertical  $\text{O}_3$  budget, detailed comparisons with photochemical models can uncover distinct weaknesses in current models and discern whether the difficulties lie in dynamical (transport) or chemical aspects of the numerical efforts (Trousdale et al., 2016).

$\text{O}_3$  vertical stratification below and above the ML-FT interface (i.e., the mixing layer height,  $h$ ) is the basis for ozone vertical exchange processes. The formation of  $\text{O}_3$  stratification is mainly due to the fact that the turbulent-convective ML and overlaying FT are usually separated by the mixing layer capping inversion, which acts as a transport barrier (Donnell et al., 2001). This barrier is indicated by steep vertical gradients of meteorological variables and chemical constituents (Petetin et al., 2018;Wyngaard and Brost, 1984;Williams et al., 2011). This means that climatological  $h$ -referenced  $\text{O}_3$  vertical distribution in the lower troposphere could provide a useful

reference for understanding vertical exchange processes and validating air quality numerical models. However, tropospheric  $O_3$  climatology is traditionally formed in a sea-level-referenced vertical coordinate system (Ding et al., 2008; Liao et al., 2021; Diab et al., 2004; Yonemura et al., 2002; Stauffer et al., 2016). Owing to day-to-day variation in the mixing layer top height, vertical stratification introduced in all individual profiles can be substantially smoothed in climatological profile when adopting the traditional vertical coordinate system. To address this issue, Petetin et al. (2018) proposed  $h$ -referenced climatology of lower-tropospheric  $O_3$  profiles based on aircraft and ozonesondes at northern mid-latitudes over 1994–2016. When adopting this  $h$ -referenced vertical coordinate system,  $O_3$  vertical stratification can be well preserved in lower-tropospheric  $O_3$  climatology, demonstrating a significant improvement in capturing possible specific features (i.e., stratification) in the  $O_3$  vertical distribution that would be smoothed with a simple average, in particular at the ML–FT interface. However, the  $h$ -referenced  $O_3$  climatology in Petetin et al. (2018) is a hemispheric-scale composite result, which cannot represent the state over polluted urban regions, including megacities.

$O_3$  pollution has long been a significant environmental issue in China, despite the 2013 Clean Air Action Plan. In recent photochemical active seasons,  $O_3$  overtook fine particles as the most important air pollutant in the three major city agglomerations: the North China Plain (NCP), the Yangtze River Delta (YRD), and the Pearl River Delta (PRD). As such, urban  $O_3$  pollution is becoming a priority for scientific research and control strategies in China (Lu et al., 2018; Wang et al., 2022b), and numerous studies have explored the spatiotemporal characteristics and formation mechanisms of surface  $O_3$  pollution, as summarized in Wang et al. (2017) and Wang et al. (2022b). Moreover, there are ongoing efforts to understand the role of vertical exchange in surface  $O_3$  pollution in China based on vertical observations from tower-based, tethered-balloon-based, unmanned-aerial-vehicle-based, aircraft-based, and lidar-based observations (Lin et al., 2010; Zhao et al., 2019; He et al., 2021; Benish et al., 2020; Zhu et al., 2020; Han et al., 2020; Chen et al., 2023). These vertically observational studies generally indicate that merging of the stable boundary layer, residual layer, and convection-driven mixing layer involves the mixing of trace gases from these different atmospheric layers, and leads to complex vertical  $O_3$  profiles. However, these existing  $O_3$  vertical observations suffer from low observation height (tower-based, tethered-balloon-based, unmanned-aerial-vehicle-based observations), short observation period (tethered-balloon-based, aircraft-based, unmanned-aerial-vehicle-based observations), and low observation accuracy (lidar-based observation), making them less able to provide a complete and accurate  $O_3$  vertical distribution for the whole lower troposphere, not to mention  $h$ -reference lower-tropospheric  $O_3$  climatology.

To our knowledge, ozonesonde represents the most accurate observation method for  $O_3$  profiles in the troposphere. Therefore, in this study, we collected ozonesonde data observed in Beijing (northern China, Fig. 1a) and Hong Kong (southern China, Fig. 1a) to investigate the  $h$ -reference  $O_3$  vertical distribution in the lower troposphere over Chinese megacities. In addition, we also considered satellite-based  $O_3$  precursor data, atmospheric composition reanalysis data, an integral method to determine the mixing layer top height  $h$ , and a photochemical indicator method to diagnose the  $O_3$  production sensitivity. The specific aims of the study were to explore (1) the degree to which lower-tropospheric  $O_3$  over megacities stratifies in the  $h$ -reference vertical coordinate system; (2) patterns in lower-tropospheric  $O_3$  profiles in the  $h$ -reference vertical coordinate system; (3) how meteorological and photochemical processes modulate  $O_3$  vertical distribution patterns in the lower troposphere; and (4) differences in the characteristics and mechanisms of lower-tropospheric  $O_3$  vertical distribution between Beijing and Hong Kong. These results of this study offer a reference for better understanding  $O_3$  pollution in urban regions.

## 2 Data and methods

## 2.1 Ozonesonde measurements

We used ozonesonde data collected by the Beijing Nanjiao Observatory (116.47°E, 39.80°N, 33 m) and Hong Kong King's Park Observatory (114.17°E, 22.31°N, 66 m) from 2000 to 2022 (Fig. 1). Beijing Nanjiao Observatory is located in southern suburban of Beijing (Fig. 1b), while Hong Kong King's Park Observatory is situated within the urban core of Hong Kong (Fig. 1c). Both sites are affected by urban traffic emissions (Fig. 1b and c).  
 135 Ozonesondes accompanied by radiosondes were regularly launched at approximately 13:30 local standard time (LST) once a week and provided high vertical resolution profiles of O<sub>3</sub>, temperature, pressure, and humidity. We excluded data from ozonesondes launched outside a time window of 12:00–15:00 LST in order to minimizes changes in mixing layer O<sub>3</sub> arising from different launch times. We interpolated the original profiles on a fixed vertical grid of 20 m vertical resolution. To reduce uncertainties associated with data gaps, we further discarded (i)  
 140 profiles with > 25% missing data between 0 and 4 km (i.e., accumulated data gaps of >  $0.25 \times 4,000 = 2,000$  m), and/or (ii) profiles with > 10 missing data points between the surface and estimated mixing layer height (i.e., accumulated data gaps of >  $10 \times 20 = 200$  m). After data exclusion, 1,897 ozonesondes were available for study: 924 soundings in Beijing and 973 soundings in Hong Kong. Figure 1d shows the monthly distribution of the available ozonesondes.

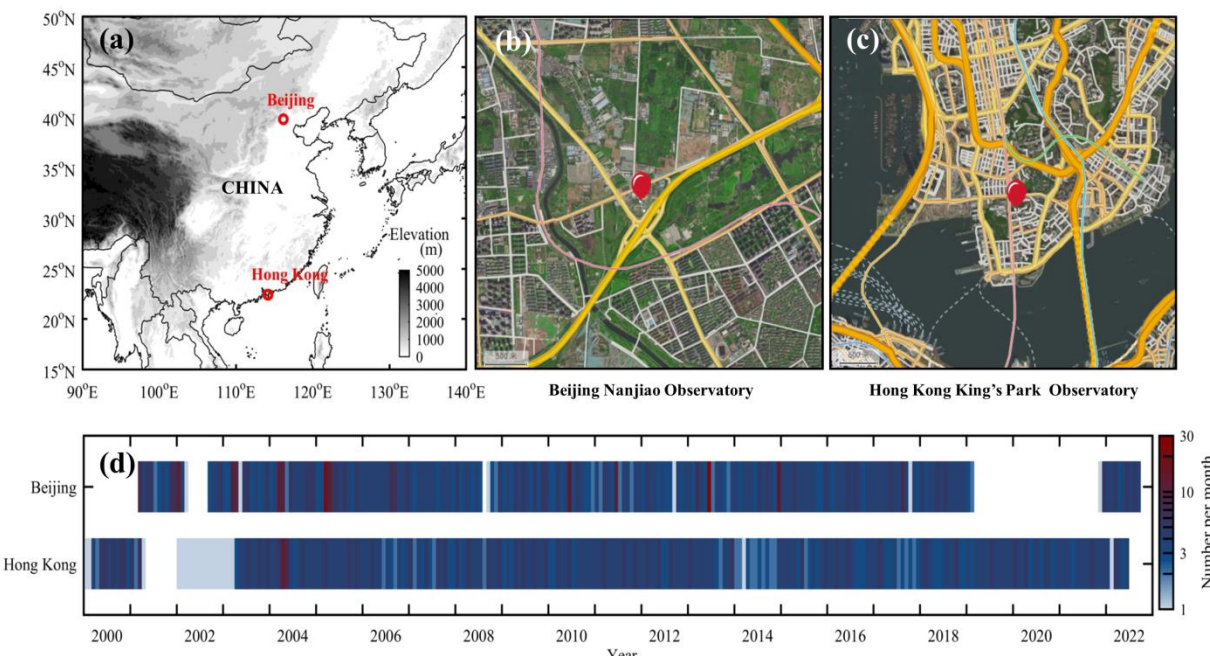


Figure 1. (a) Coordinates and surrounding environments of ozonesonde sites at (b) Beijing Nanjiao Observatory and (c) Hong Kong King's Park Observatory. (d) Monthly distribution of the available ozonesonde observations. Map image is © Amap.

## 2.2 Meteorological and atmospheric composition reanalysis

The fifth generation reanalysis (ERA5) data from the European Center for Medium-Range Weather Forecasts (ECMWF) were used to characterize synoptic meteorological conditions. The meteorological variables include geopotential height and horizontal wind vector at 850 hPa, downward ultraviolet radiation at the surface. ERA5 is generated by 4-D variational data assimilation of the ECMWF's Integrated Forecast System and predictions from the CF41R2 model (Hersbach et al., 2020). It has a spatial resolution of  $0.25^\circ \times 0.25^\circ$ . Besides, pressure-level CH<sub>2</sub>O and NO<sub>2</sub> data from the fourth-generation ECMWF Atmospheric Composition Reanalysis (EAC4) were also used to characterize O<sub>3</sub> precursor concentrations and diagnose vertical O<sub>3</sub> production sensitivity. The EAC4  
 155

combines model data with global satellite observations into a complete and consistent dataset using a model of the atmosphere based on the laws of physics and chemistry (Inness et al., 2019). It was available at 3-h resolution for a horizontal resolution of  $0.75^\circ \times 0.75^\circ$  and a vertical resolution of 7 layers below 700 hPa (1000, 950, 925, 900, 850, 800, and 700 hPa). All abovementioned reanalysis data at 06:00 UTC from 2003 onwards were used to support our interpretation of sonde-based  $O_3$  vertical distribution.

### 2.3 Determination of mixing layer top height $h$

Several approaches have been developed to estimate  $h$  based on the gradient variation of individual atmospheric variables from radiosonde data (Seidel et al., 2010), including temperature ( $T$ ), potential temperature ( $\theta$ ), relative humidity ( $RH$ ), specific humidity ( $q$ ), and atmospheric refractivity ( $N$ ). However, there are substantial differences in the existing methods. Wang and Wang (2014) proposed a three-step method to integrate temperature, humidity, and cloud data to generate a consistent estimate of  $h$  from radiosonde profiles: Step 1, identify the height ( $h_0$ ) that best meets the individual criteria for different atmospheric variables; step 2, derive the location of the cloud; and step 3, determine a consistent mixing layer height ( $h_{con}$ ). We adopted this integral method to determine the mixing layer heights in Beijing and Hong Kong. Five atmospheric variables, namely,  $T$ ,  $\theta$ ,  $RH$ ,  $q$ , and  $N$ , were used. Among them,  $T$  and  $RH$  were measured by radiosonde, and the other variables were calculated from  $T$ ,  $RH$ , and atmospheric pressure (Seidel et al., 2010). The upper limit of  $h$  was set to 4 km.

### 2.4 $h$ -referenced vertical distribution and classification

Once the mixing layer height  $h$  was determined, all profiles were expressed in the  $z/h$  vertical coordinate system, where  $z$  is the actual altitude. In practice, atmospheric variables were interpolated along  $z/h$  values ranging between 0 (the surface) and 2 ( $2 \times h$ ) with a vertical resolution of 0.05 (i.e., 41 altitude levels). For instance, if  $h$  on a specific profile was 1,000 m, the resampled profile extended from 0 to 2000 m with bins of 50 m. Hereafter, this type of vertical profile is denominated as a mixing-layer-height-referenced (i.e.,  $h$ -referenced) profile. In this  $z/h$  vertical coordinate system, mixing-layer  $O_3$  was denominated as  $MLO_3$  and free-tropospheric  $O_3$  was denominated as  $FTO_3$ . Based on Student's  $t$  test, we further classified individual  $h$ -referenced  $O_3$  profiles into three distinct patterns:  $MLO_3$ -dominated (mean  $MLO_3$  significantly higher than mean  $FTO_3$  at a significance level of 0.01);  $FTO_3$ -dominated (mean  $MLO_3$  significantly lower than mean  $FTO_3$  at a significance level of 0.01); and uniform distribution (no significant differences between the means of  $MLO_3$  and  $FTO_3$ ).

### 2.5 Diagnosis of ozone production sensitivity

$O_3$  is photochemically generated when its precursors (e.g.,  $NO_x$  and VOCs) are abundant in the presence of sunlight (Seinfeld and Pandis, 2016). Owing to complex chemical mechanisms and regional differences in emissions and meteorology, the relationship between  $O_3$  and its precursors involves highly non-linear interactions (Jin et al., 2020). Under high VOC and low  $NO_x$  conditions,  $O_3$  production is not sensitive to VOCs, but is positively correlated to  $NO_x$  (i.e., a  $NO_x$ -sensitive regime). Under low VOC and high  $NO_x$  conditions,  $O_3$  production tends to increase with VOC growth or  $NO_x$  reduction (i.e., VOC-sensitive regime). In this study, the  $CH_2O/NO_2$  ratio (FNR) was used as the photochemical indicator to diagnose  $O_3$  production sensitivity. An inherent challenge of this diagnosis approach is that FNR thresholds marking the VOC- $NO_x$  transition regime are likely distinct from region to region (Jin et al., 2020). For the NCP region (including Beijing), Li et al. (2021) diagnosed the transition regime as occurring when FNR ranges from 1.2 to 2.1; for the PRD region (including Hong Kong), Liao et al. (2021) diagnosed the transition regime as occurring when FNR ranges from 1.0 to 1.5. Ratios below and above these ranges indicate VOC-limited  $O_3$  production and  $NO_x$ -limited regimes, respectively. These localized FNR thresholds were adopted in this study to diagnose  $O_3$  production sensitivity.

### 3 Results and discussion

#### 3.1 Lower-tropospheric ozone climatology

Figure 2 shows the traditional lower tropospheric O<sub>3</sub> climatology of Beijing and Hong Kong. Seasonal results are averaged from ozonesonde profiles collected in spring (M–A–M), summer (J–J–A), autumn (S–O–N), and winter (D–J–F). There is a typical summer-high-winter-low seasonality in lower tropospheric O<sub>3</sub> over Beijing, with the highest O<sub>3</sub> concentrations in June. Such seasonality is broadly similar to previous tropospheric O<sub>3</sub> climatology based on lesser O<sub>3</sub> profiles in Beijing (Ding et al., 2008; Zhang et al., 2021). In photochemical active months (May–August), high-concentration O<sub>3</sub> is photochemically produced throughout the lower troposphere, particularly in the mixing layer, causing an isolated O<sub>3</sub>-peak area (> 100 ppbv) near the upper mixing layer. In other months, strong urban NO-titration accompanied by weak O<sub>3</sub> production causes a positive vertical gradient of O<sub>3</sub> concentration in the lower troposphere; the average vertical gradient of O<sub>3</sub> reaches a maximum in winter.

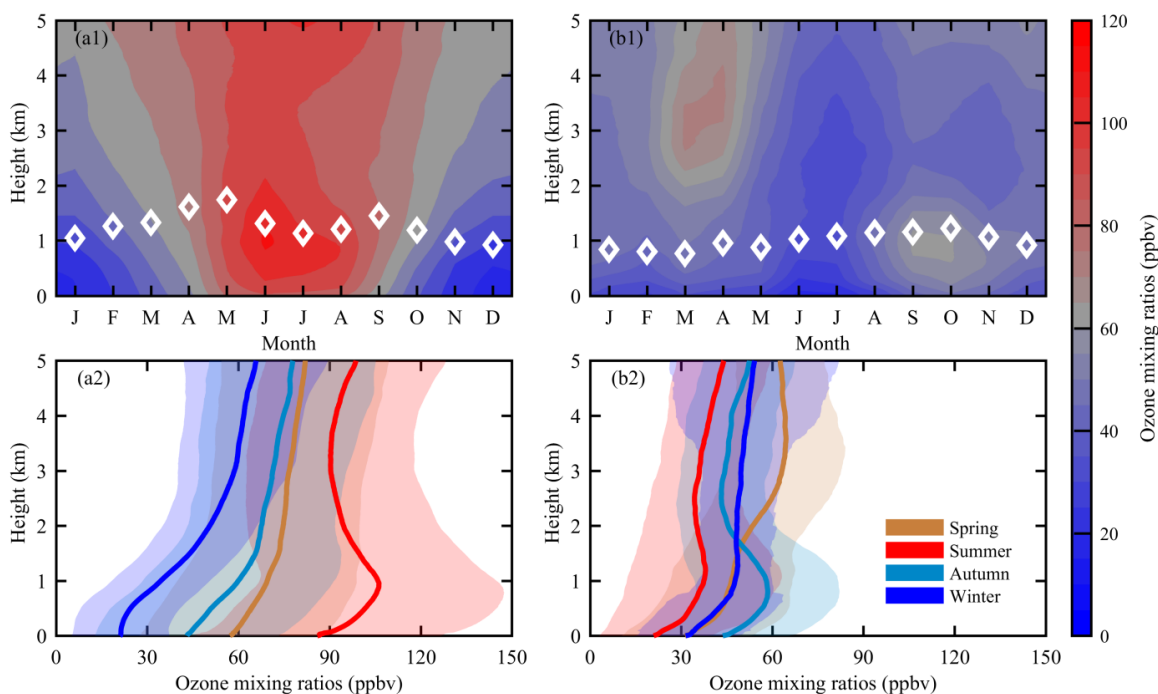


Figure 2. Lower tropospheric ozone vertical distribution over (a) Beijing and (b) Hong Kong. (1) Monthly variation (2) Seasonal variation. The white diamonds in (1) represent the monthly mean mixing layer height. The shaded areas in the lower panels denote the standard deviation.

Lower tropospheric O<sub>3</sub> climatology in Hong Kong is remarkably different from that in Beijing. In particular, lower tropospheric O<sub>3</sub> is low in the summertime (< 40 ppbv). Similar O<sub>3</sub> minima have been reported in other subtropical cities in Eastern Asia, such as Hanoi and Naha (Liao et al., 2021; Oltmans et al., 2004; Ogino et al., 2013) and likely reflect the influence of the Asian summer monsoons, which bring maritime air with low O<sub>3</sub> northward from the tropical Pacific to subtropical regions. Although Beijing is also impacted by the Asian summer monsoons, these ocean-sourced air masses become enriched with O<sub>3</sub> precursors while passing over polluted eastern China, leading to an accumulation of O<sub>3</sub> over Beijing. Interestingly, there are two isolated areas of O<sub>3</sub> enhancement over Hong Kong, those in the lower free troposphere (~3.5 km) from March to April and in the upper mixing layer (~0.8 km) in autumn. The former is attributed to long-range transport of wildfire-related O<sub>3</sub> production in the upwind Indochina Peninsula; the latter results from local O<sub>3</sub> production via photochemical reactions under hot and dry

weather conditions in autumn (Liao et al., 2021).

230

### 3.2 Mixing-layer-height-referenced ozone vertical distribution

We investigated the climatological vertical stratification of  $O_3$  below and above the ML-FT interface (i.e., mixing layer height  $h$ ) over Beijing and Hong Kong (Fig. 3). This  $h$ -referenced  $O_3$  climatology provides an additional dimension (further categorization by mixing layer height) not available in traditional vertical ozone profile climatology. The significant disparity between the  $h$ -referenced  $O_3$  climatology (Fig. 3) and traditional  $O_3$  climatology (Fig. 2) illustrates how much information is lost using simple ozonesonde averages. For example, the  $h$ -referenced  $O_3$  profiles show a clear inflection (or discontinuity) at the interface between the ML and FT ( $z/h=1$ ), which is not apparent in the traditional  $O_3$  climatology. These results reflect the fact that mixing-layer capping inversion acts as an effective although porous geophysical barrier that limits vertical exchange between the ML and FT, leading to distinct  $O_3$  levels on either side.

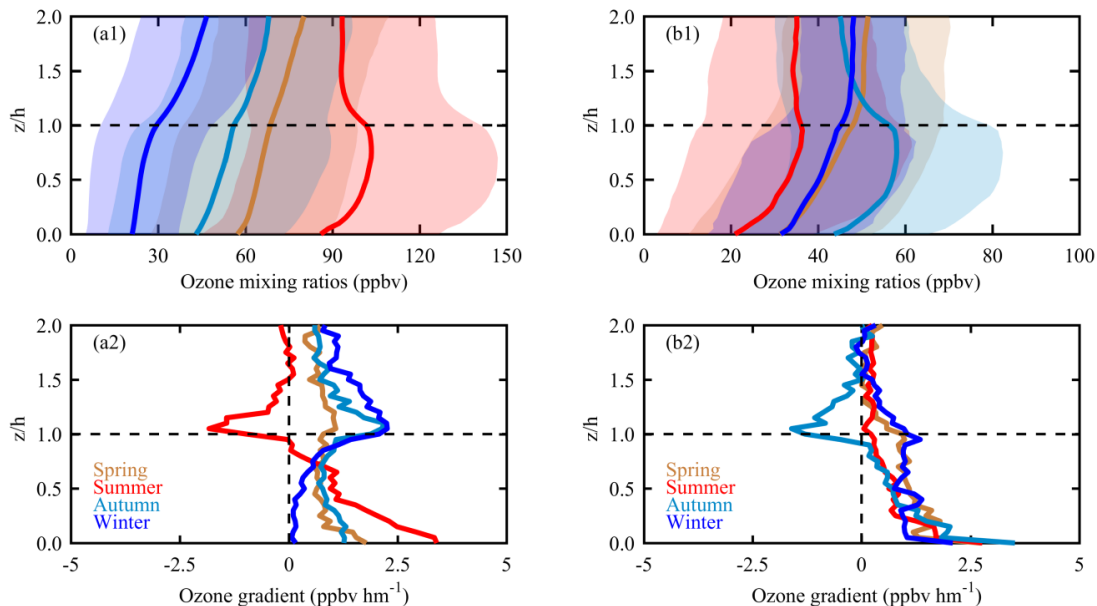


Figure 3. Mixing-layer-height-referenced ozone vertical distribution over (a) Beijing and (b) Hong Kong. (1) Ozone mixing ratio profile. (2) Ozone gradient profile. The shaded areas in the upper panels denote the standard deviation.

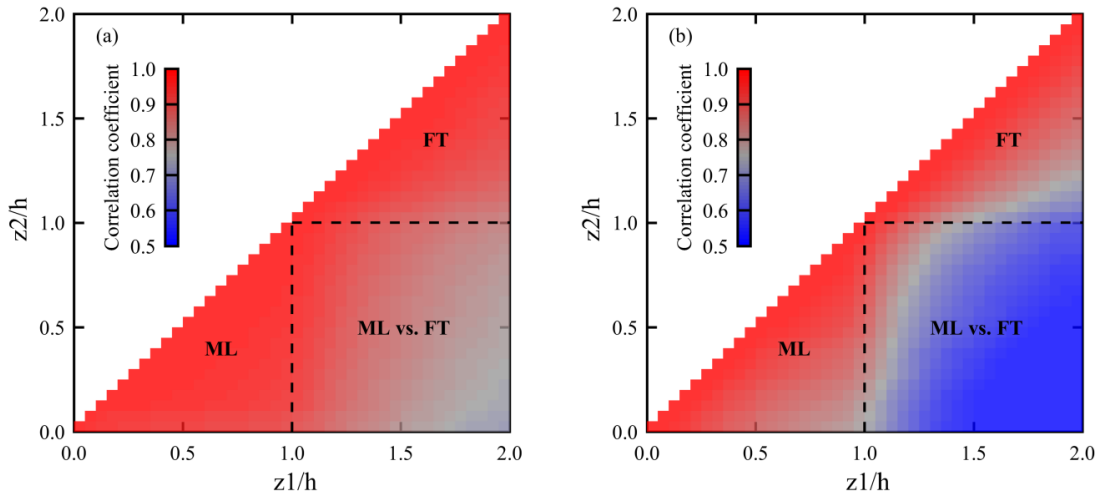
245

In Beijing, seasonal  $O_3$  profiles in autumn, winter, and spring present a low-ML/high-FT vertical distribution pattern with  $O_3$  mixing ratios that increase with altitude throughout the lower troposphere and variable vertical gradients depending on season and altitude. Generally, the strongest gradients are observed either close to the surface or near the ML-FT interface. Near the surface, they are likely due to strong  $O_3$  titration by NO emitted from urban traffic (Karl et al., 2023). Near the ML-FT interface, they are likely attributable to the barrier effect of mixing-layer capping inversion. The  $O_3$  gradients gradually decrease with altitude above the ML-FT interface; below the interface, they slightly decrease with altitude in spring and autumn but gradually increase with altitude in winter. Winter  $O_3$  gradients are almost zero in the surface layer ( $z/h < 0.4$ ), reflecting strong titration that often causes  $O_3$  to be almost completely depleted in the lower ML. In summer, the averaged  $O_3$  profile exhibits a sickle-shape pattern, with a marked drop in concentrations from the upper ML to the lower FT. Summer  $O_3$  gradients quickly decrease with altitude inside the ML and eventually become negative near the ML-FT interface. The maximum negative gradient (-2.2 ppbv  $hm^{-1}$ ) occurs just above the mixing layer top height. In Hong Kong, the averaged  $O_3$  profiles in winter and spring present low-ML/high-FT vertical distribution, similar to Beijing. However, the autumn averaged  $O_3$  profile shows a sickle-shape pattern, similar to the summer profile in Beijing. In contrast,

the summer averaged  $O_3$  profile in Hong Kong displays a transitional feature from spring to autumn, characterized  
260 by a weak  $O_3$  peak just below the ML–FT interface. Compared with Beijing, the  $O_3$  gradients in Hong Kong vary  
across a smaller range; however, they are commonly sharper in the surface layer.

For both Beijing and Hong Kong, the highly variable  $O_3$  gradients in the ML confirm that the well-mixed ML  
265 remains a large exception for  $O_3$ , even on summer afternoons when vertical turbulent mixing is expected to be  
strongest. In particular, the increasing  $O_3$  with altitude in the lower ML indicates that strong photochemistry and  
270 vertical mixing on summer afternoons is insufficient to quickly compensate for  $O_3$  titration consumption  
( $NO + O_3 \rightarrow NO_2$ ) in the surface layer, where NO is largely emitted by urban traffic. A previous study indicated that  
275  $MLO_3$  evolution in urban areas adheres to vertical physiochemical circulation involving multiple reactions in the  
 $O_3$ –NO– $NO_2$  triad (Tang et al., 2017). NO emissions react with  $O_3$  to generate  $NO_2$  near the ground, which is then  
280 transported vertically to the upper ML;  $O_3$  is generated by  $NO_2$  photolysis in the upper ML and is then transported  
down to the surface layer to compensate for the loss by NO titration. In this process, the titration process is thought  
to drive the downward flux of  $O_3$  into the urban roughness layer (Karl et al., 2023). Under favorable weather  
285 conditions, high-concentration  $MLO_3$  production can greatly modify the vertical profile of  $O_3$  from the more  
customary low-ML/high-FT vertical distribution to a high-ML/low-FT vertical distribution. This modification is  
thought to be episodic in low-emission cities (e.g., Frankfurt; (Petetin et al., 2016); in such cities, the vertical  
290 structure of averaged  $O_3$  profiles in the photochemical active season (e.g., summer) remains low-ML/high-FT the  
same throughout the year (Petetin et al., 2018). However, in high-emission megacities (e.g., Beijing and Hong  
Kong), photochemistry-driven modification can be expected to be common during in the photochemical active  
295 season (summer in Beijing and autumn in Hong Kong), eventually causing a seasonal sickle-shape  $O_3$  profile in the  
lower troposphere. These seasonal differences in lower tropospheric  $O_3$  profiles imply that the aforementioned  
transport barrier to vertical exchange has different connotations, typically changing from a ML-to-FT detrainment  
barrier in summer (autumn) to a FT-to-ML entrainment barrier in other seasons in Beijing (Hong Kong).

The vertical autocorrelation of  $O_3$  in the  $z/h$  vertical coordinate system was further analyzed to investigate the  
285 links between the ML and FT. Based on all individual  $O_3$  profiles, we calculated the correlation coefficients of  $O_3$   
between the different pairs of  $z/h$  altitude levels. The obtained  $O_3$  vertical autocorrelation matrix is shown in Figure  
4. Within both the ML ( $z/h$  between 0 and 1) and FT ( $z/h$  between 1 and 2), we found strong correlations (usually  $> 0.90$ , mean of 0.97 in Beijing;  $> 0.85$ , mean of 0.91 in Hong Kong). However, the correlations between the two  
290 atmospheric compartments (ML vs. FT) decreased quickly with vertical distance, with means of 0.84 in Beijing and  
0.60 in Hong Kong. In general, correlations in Hong Kong were found to be weaker than those in Beijing. This can  
be explained by two possible reasons. (i) Hong Kong is a coastal city, where clean maritime air and polluted  
295 continental air can dominate at different altitudes (e.g., sea-land breeze); therefore, distinct air mass sources can  
weaken the correlation of  $O_3$  between different altitude levels. (ii) Hong Kong is located in humid zone, where  
surface sensible heat is relatively weaker than that in semi-humid zones (e.g., Beijing); therefore, weak turbulent  
convection causes weak mixing of  $O_3$  in the vertical direction (Xu et al., 2021). The iso-correlation contours in both  
megacities present a “W” shape along the diagonal direction, with the inflection point at  $z/h = 1$ . This is consistent  
with northern mid-latitude findings in Petetin et al. (2018), indicating that stratification occurs most commonly at  
the ML–FT interface.



300 Figure 4. Auto-correlation of ozone mixing ratios between different  $z/h$  altitude levels over (a) Beijing and (b) Hong Kong. Dashed lines separate three areas involving correlation within the mixing layer (ML), within the free troposphere (FT), and between the mixing layer and free troposphere (ML vs. FT).

305 Both surface concentration and vertical distribution of  $O_3$  are highly variable at the synoptic scale and can greatly depart from standard climatology depending on meteorological conditions and the availability of  $O_3$  precursors. Based on Student's  $t$  test, all individual  $h$ -referenced  $O_3$  profiles were further classified into three typical patterns to investigate synoptic climatology of lower tropospheric  $O_3$  in Beijing and Hong Kong. The statistical results indicate that the  $FTO_3$ -dominated pattern occurs most frequently in both megacities. The respective occurrence frequencies of  $FTO_3$ -dominated, uniform, and  $MLO_3$ -dominated distributions were 69%, 11%, and 20% in Beijing, and 54%, 21%, and 25% in Hong Kong, respectively. Figure 5 shows the composite of  $O_3$  (gradient) profiles according to the different  $O_3$  profile patterns in Beijing and Hong Kong. In the  $FTO_3$ -dominated pattern, averaged  $FTO_3$  concentrations are 61.6 ppbv in Beijing and 44.9 ppbv in Hong Kong, which are 15 and 13 ppbv higher than the averaged  $MLO_3$  concentrations in the respective cities. Such concentration differences between  $FTO_3$  and  $MLO_3$  cause a sharp positive gradient of  $O_3$  near the ML-FT interface ( $2.3 \text{ ppbv hm}^{-1}$  in Beijing and  $1.8 \text{ ppbv hm}^{-1}$  in Hong Kong). For the  $MLO_3$ -dominated pattern, averaged  $MLO_3$  concentrations are 109.8 ppbv in Beijing and 62.2 ppbv in Hong Kong,  $\sim 18$  ppbv higher than the averaged  $FTO_3$  concentrations in both cities, causing a steep negative gradient of  $O_3$  near the ML-FT interface ( $-4.3 \text{ ppbv hm}^{-1}$  in Beijing and  $-3.8 \text{ ppbv hm}^{-1}$  in Hong Kong). For the uniform distribution, despite no significant difference in the means of  $MLO_3$  and  $FTO_3$ , the composited  $O_3$  profile shows an "S" shape pattern with a slightly negative gradient (approximately  $-1.0 \text{ ppbv hm}^{-1}$ ) 310 near the ML-FT interface.

315

320

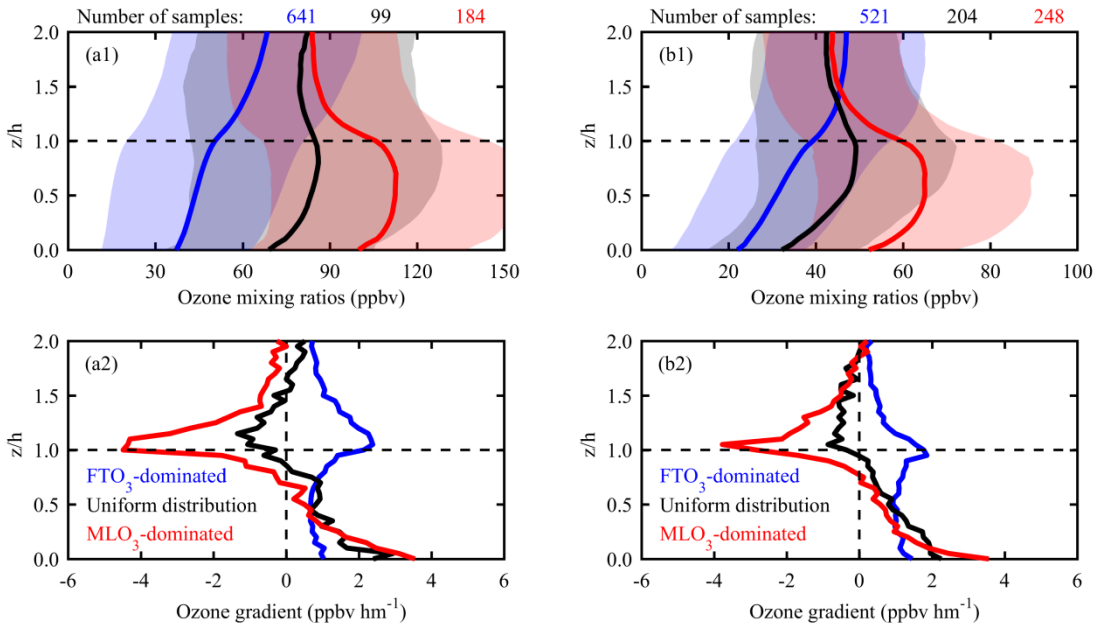


Figure 5. Composites of (1)  $h$ -referenced ozone profiles and (2)  $h$ -referenced ozone gradient profiles according to different patterns in (a) Beijing and (b) Hong Kong. The shaded areas in the upper panels denote the standard deviation.

325

Figure 6 shows occurrence frequencies of the three distinct  $O_3$  profile patterns in different seasons and mixing layer height bins. In Beijing, while the  $FTO_3$ -dominated pattern prevails in winter (94.2%), autumn (79.1%), and spring (75.3%), the  $MLO_3$ -dominated pattern prevails in summer (46.3%). In Hong Kong, the  $FTO_3$ -dominated pattern occurs frequently in spring (67.7%), winter (65.8%), and summer (55.8%), and the  $MLO_3$ -dominated pattern prevails in autumn (55.1%). Such frequent occurrence of  $MLO_3$ -dominated patterns confirms our theory that the  $MLO_3$ -dominated pattern is common rather than episodic in the photochemical active season of high-emission Chinese megacities. In contrast, the occurrence dependence of  $O_3$  profile patterns on mixing layer height is not as strong as that on season. The  $FTO_3$ -dominated pattern prevails in most  $h$  bins, particularly in Beijing. Nevertheless, the  $MLO_3$ -dominated pattern is still relatively more frequent in the  $h$  bin between 1.0 and 2.0 km (27.3% in Beijing and 36.7% in Hong Kong) than in lower and higher  $h$  bins. This is to some degree consistent with the findings of Zhao et al. (2019), who revealed that moderate mixing layer height is usually accompanied by very favorable meteorological (moderate RH and high temperature) and photochemical ( $NO_x$ -VOC transition regime) conditions for high-concentration  $MLO_3$  production.

340

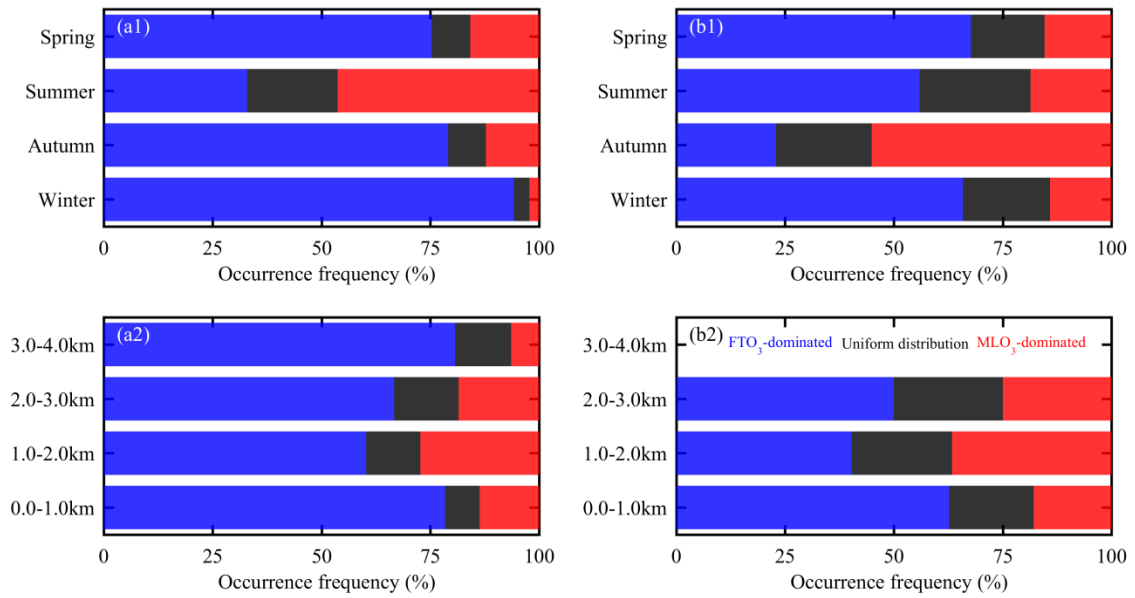


Figure 6. Occurrence frequencies of three  $h$ -referenced ozone profile patterns according to (1) season and (2) mixing layer height bins in (a) Beijing and (b) Hong Kong (in Hong Kong, no case is found for  $h > 3.0$  km).

345

### 3.3 Mechanistic understanding of distinct ozone profile patterns in polluted seasons

350

This section explores the causal mechanisms of distinct  $O_3$  profile patterns in summer of Beijing and autumn of Hong Kong. These two seasons represent the typical ozone-pollution season in individual megacities (Fig. 2). Meanwhile, the days in these two seasons are usually alternately controlled by different  $O_3$  profile pattern, rather than overwhelmingly controlled by single  $O_3$  profile pattern, i.e.,  $FTO_3$ -dominated pattern (Fig. 6). Therefore, the results focusing on these two seasons will provide a more in-depth understanding of ozone pollution mechanisms through comparison among the different  $O_3$  profile patterns.

360

365

Figure 7 shows the composited  $h$ -referenced  $O_3$  profiles and  $MLO_3$  concentrations according to different  $O_3$  profile patterns in summer of Beijing and autumn of Hong Kong. It can be seen that the  $MLO_3$  concentrations present a wide-range variability across the different  $O_3$  profile patterns, while  $O_3$  in the FT part shows a similar concentration, especially in the uppermost part of  $h$ -referenced lower troposphere, indicating that downward transport of  $O_3$ -rich air masses from high altitudes such as stratosphere is not the main factor working to shape the distinct lower-tropospheric  $O_3$  profile patterns. Given the  $O_3$  photochemistry is active in the mixing layer, the wide-range  $MLO_3$  variability indicates that the distinct lower-tropospheric  $O_3$  profile patterns are mainly attributed to varying  $MLO_3$  production, which is modulated by multi-scale meteorology and ozone precursors. In  $MLO_3$ -dominated pattern, the medians of  $MLO_3$  concentrations are 117.5 ppbv in Beijing and 61.9 ppbv in Hong Kong, far higher than the corresponding values (66.0 ppbv in Beijing and 33.0 ppbv in Hong Kong) in  $FTO_3$ -dominated patterns. This indicates that  $MLO_3$ -dominated pattern has a very strong  $O_3$  production through photochemical reaction, whereas  $FTO_3$ -dominated pattern corresponds to a weak  $O_3$  production or even a strong  $O_3$  titration ( $NO+O_3 \rightarrow NO_2$ ).

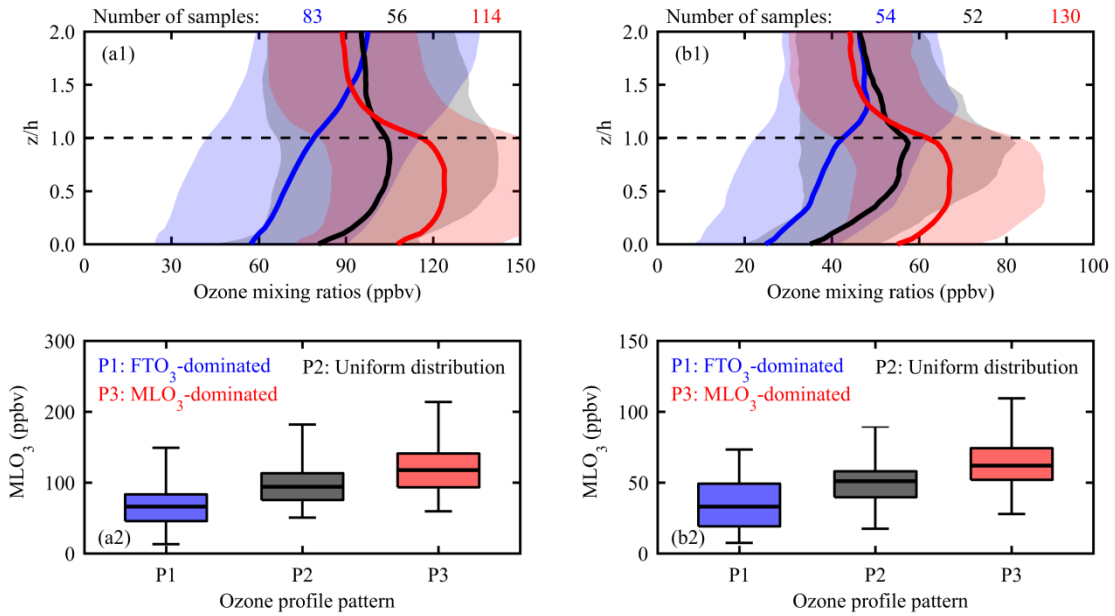


Figure 7. (1) Composited  $h$ -referenced ozone profiles and (2)  $\text{MLO}_3$  concentrations according to different ozone profile patterns in (a) summer of Beijing and (b) autumn of Hong Kong. The shaded areas in the upper panels denote the standard deviation. The box-whisker plots in the lower panels denote the  $\text{MLO}_3$  concentrations of 2.5, 25, 50, 75, 97.5 percentiles. The digits at the upper of plots denote the sample numbers in each of patterns.

### 3.3.1 Meteorological interpretations

Synoptic meteorological conditions play an important role in controlling lower-tropospheric ozone variability (Kalabokas et al., 2013; Kalabokas et al., 2015; Stauffer et al., 2017). Figure 8 shows the composited large-scale geopotential height and horizontal wind vector at 850 hPa and downward ultraviolet radiation at the surface according to different  $\text{O}_3$  profile patterns in summer of Beijing and autumn of Hong Kong.

In summer, northern China is controlled by continental thermal low-pressure system with prevailing of southerly flows in the North China Plain. The southerly flows are favorable for transporting ozone and its precursors from central Eastern China to Beijing (Liao et al., 2023), resulting in ozone production and accumulation in the presence of strong ultraviolet radiation. From the  $\text{FTO}_3$ -dominated to  $\text{MLO}_3$ -dominated pattern, the low-pressure system is gradually weakened. This change leads to an inhabitation of convective cloud formation, favoring downward ultraviolet radiation. In Fig. 8a, there is a slight increase in the downward ultraviolet radiation over northern China from the  $\text{FTO}_3$ -dominated to  $\text{MLO}_3$ -dominated pattern, suggesting a tendency toward more favorable photochemical condition. In autumn, southern China is controlled by weak high-pressure system. From the  $\text{FTO}_3$ -dominated to  $\text{MLO}_3$ -dominated pattern, the high-pressure system is gradually strengthened, leading to a significant wind direction change from Pacific-originating easterly flows to continent-originating northeasterly flows over Hong Kong and its surrounding region. The wind direction change causes increasing influence of regional transport of ozone precursors originating from eastern China (Ding et al., 2013). Meanwhile, the strengthened high-pressure system suppresses convective cloud formation, resulting in a significant increase in downward ultraviolet radiation (from  $180 \text{ kJ m}^{-2}$  to  $230 \text{ kJ m}^{-2}$ ) over Hong Kong and its surrounding region.

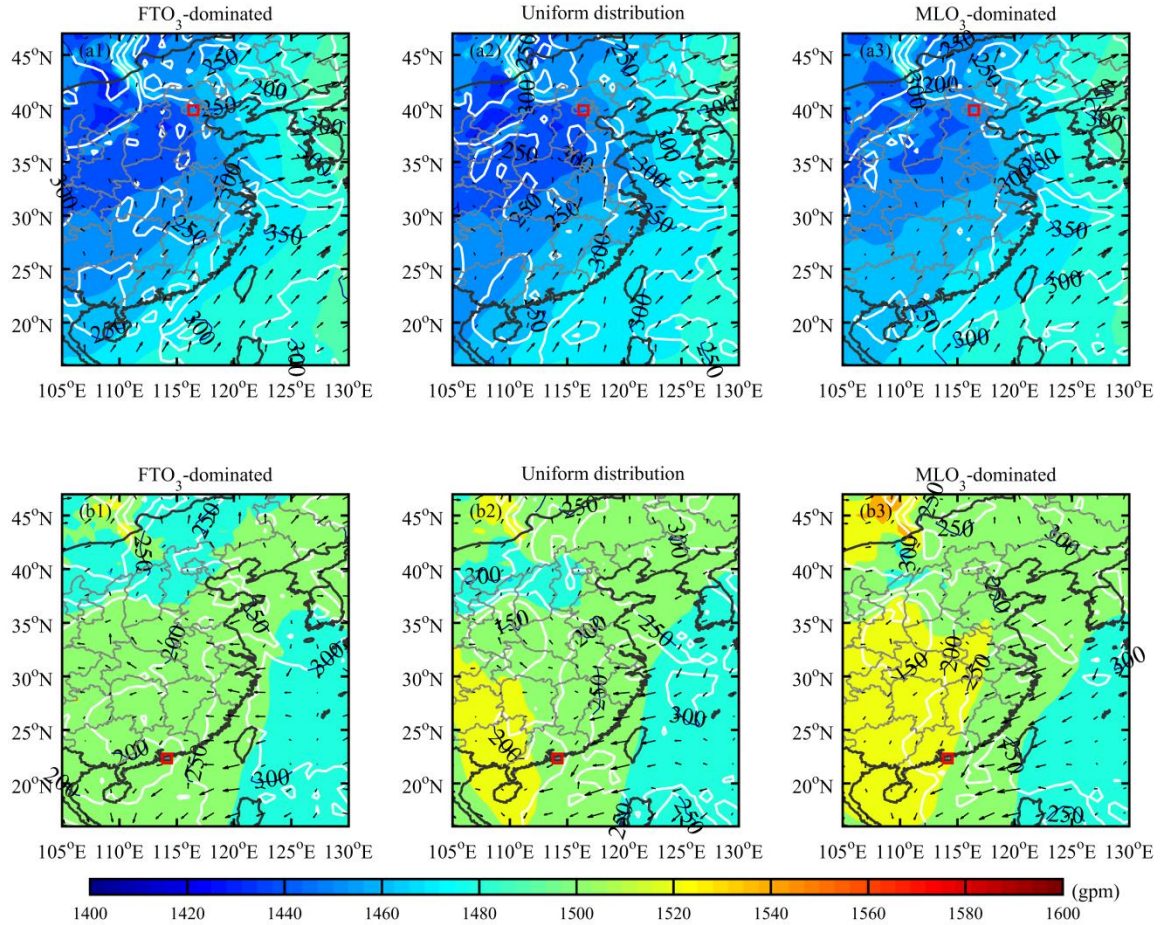


Figure 8. Composited large-scale meteorology, including geopotential height and horizontal wind vector at 850 hPa and downward ultraviolet radiation at the surface (contour,  $\text{kJ m}^{-2}$ ), according to different ozone profile patterns in (a) summer of Beijing and (b) autumn of Hong Kong. The red boxes indicate the locations of Beijing and Hong Kong.

In contrast to large-scale meteorology, local meteorology exerts more direct influences on local ozone production and accumulation. The  $h$ -referenced profiles of potential temperature ( $\theta$ ), relative humidity (RH), and wind speed (WS) according to different  $\text{O}_3$  profile patterns in summer of Beijing and autumn of Hong Kong are shown in Figure 9. Near the surface ( $z/h < 0.1$ ), potential temperature decreases with altitude in both megacities, indicating a shallow superadiabatic layer due to daytime surface radiation heating. In other parts of the ML, potential temperature profiles are neutral adiabatic (small positive gradient) due to afternoon convection (Stull, 1988). However, potential temperature in the FT ( $z/h > 1.0$ ) increases with altitude with a larger positive gradient than that in the ML. Particularly, there is a sharp increase in potential temperature at the ML-FT interface where positive vertical gradients reach  $1.0 \text{ }^{\circ}\text{C hm}^{-1}$  on average. This large gradient is indicative of strong mixing layer capping thermal inversion. However, the maximum gradient values are almost identical among the different  $\text{O}_3$  profile patterns, suggesting that capping inversion acts as a transport barrier to suppress  $\text{O}_3$  vertical exchange but is not responsible for the different directions of vertical exchange (i.e., FT-to-ML entrainment or ML-to-FT detrainment). Overall, no significant structural change is found in the averaged  $\theta$  profiles among the different patterns. Similar to the  $\theta$  profiles, the RH and WS profiles share an analogous vertical structure among different  $\text{O}_3$  profile patterns in both megacities.

Without considering the vertical structure, values of aforementioned meteorological variables usually differ largely among the different  $O_3$  profile patterns. From the  $FTO_3$ -dominated to  $MLO_3$ -dominated pattern, there is a significant increase in potential temperature value in Beijing. The high temperature favors high-concentration ozone production in the  $MLO_3$ -dominated pattern. Previous studies have indicated that high temperature not only increases the  $O_3$  production rate (Wang et al., 2022a), but also strengthens the volatilization rate of  $O_3$  precursors, particularly biomass VOC emissions (Duncan et al., 2009). However, there are no significant temperature differences between  $FTO_3$ -dominated and  $MLO_3$ -dominated pattern in Hong Kong, indicating an insensitivity of Hong Kong's ozone production to air temperature. Turning to relative humidity, it has a significant decrease from  $FTO_3$ -dominated pattern to  $MLO_3$ -dominated pattern in both megacities. Given that humid air tends to suppress photochemical reactions (Yu, 2019), the lower RH in the  $MLO_3$ -dominated pattern favors ozone photochemical production. In contrast to RH, the cross-pattern WS profile change shows some differences between Beijing and Hong Kong. For example, on  $MLO_3$ -dominated days, WS is low in Beijing but high in Hong Kong. The high WS conditions indicate that regional transport play an important role in  $O_3$  pollution in Hong Kong. From above analyses a common meteorological factor leading to the  $MLO_3$ -dominated pattern in both megacities is low RH.

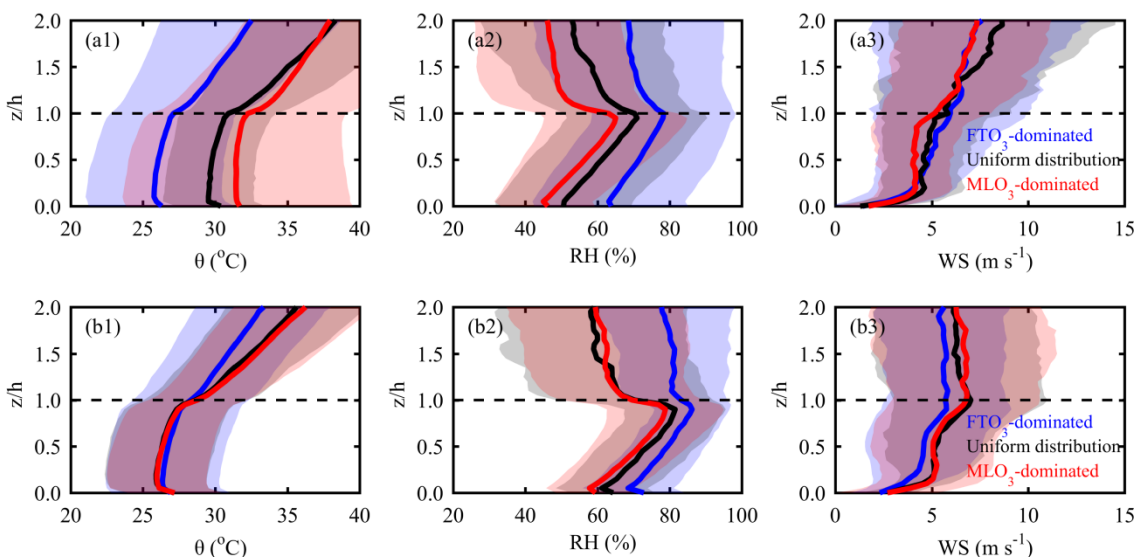


Figure 9. Composited  $h$ -referenced profiles of (1) potential temperature, (2) relative humidity, and (3) wind speed according to different ozone profile patterns in (a) summer of Beijing and (b) autumn of Hong Kong. The shaded areas denote the standard deviation.

### 3.3.2 Photochemical interpretations

Figure 10 shows composited vertical distributions of EAC4-based  $CH_2O$  and  $NO_2$  concentrations according to the different  $O_3$  profile patterns in summer of Beijing and autumn of Hong Kong. There are significant higher precursor concentrations in Beijing than that in Hong Kong, particularly above the surface layer. This partly explains the higher ozone concentration in Beijing. No matter  $CH_2O$  and  $NO_2$ , its concentration decreases with altitude in both megacities. By comparison, the vertical gradient of ozone precursors in Hong Kong is significantly larger than that in Beijing. For the different ozone precursors, the vertical gradient of  $CH_2O$  is significant smaller than that of  $NO_2$  in the ML part (below 850 hPa). For example, the  $NO_2$  concentration decreases 50-75% (80-85%) from the near surface to 900 hPa in Beijing (Hong Kong), while the corresponding  $CH_2O$  concentration just decreases approximately 30% (60%). These vertical characteristics of EAC4-based ozone precursors are consistent with those previous observations (Chi et al., 2018; Lin et al., 2022; Liu et al., 2023).

From the  $\text{FTO}_3$ -dominated to  $\text{MLO}_3$ -dominated pattern,  $\text{CH}_2\text{O}$  increases throughout the lower troposphere (up to 700 hPa) in Beijing with a maximum increment in the upper ML (~900 hPa). The maximum  $\text{CH}_2\text{O}$  increment near the mixing layer top may be explained by northward transport of VOC emissions in eastern China and high-elevation biogenic VOC emissions in the western mountains (i.e., Taihang Mountains). In contrast to  $\text{CH}_2\text{O}$ ,  $\text{NO}_2$  decreases in the ML part (below 900 hPa), especially in the surface layer (1000 hPa). For example, surface  $\text{NO}_2$  concentration is approximately  $14 \times 10^{-9} \text{ kg kg}^{-1}$  in the  $\text{FTO}_3$  pattern, but decreases to approximately  $9 \times 10^{-9} \text{ kg kg}^{-1}$  in the  $\text{MLO}_3$  pattern. The cross-pattern change of  $\text{O}_3$  precursors in Hong Kong nearly follows the same characteristic as that in Beijing (i.e., increase of  $\text{CH}_2\text{O}$  and decrease of  $\text{NO}_2$  from  $\text{FTO}_3$ -dominated to  $\text{MLO}_3$ -dominated), but with a significantly smaller change amplitude. This difference is likely attributable to temperature-driven precursor changes. In Beijing, the cross-pattern temperature change is very significant. Higher temperature in the  $\text{MLO}_3$ -dominated pattern tends to trigger the release of VOC emissions, causing higher  $\text{CH}_2\text{O}$  concentrations, and to improve the photolysis of  $\text{NO}_2$ , causing lower  $\text{NO}_2$  concentrations. However, the cross-pattern temperature change is insignificant in Hong Kong, leading to small change amplitude of ozone precursors among the different  $\text{O}_3$  profile patterns.

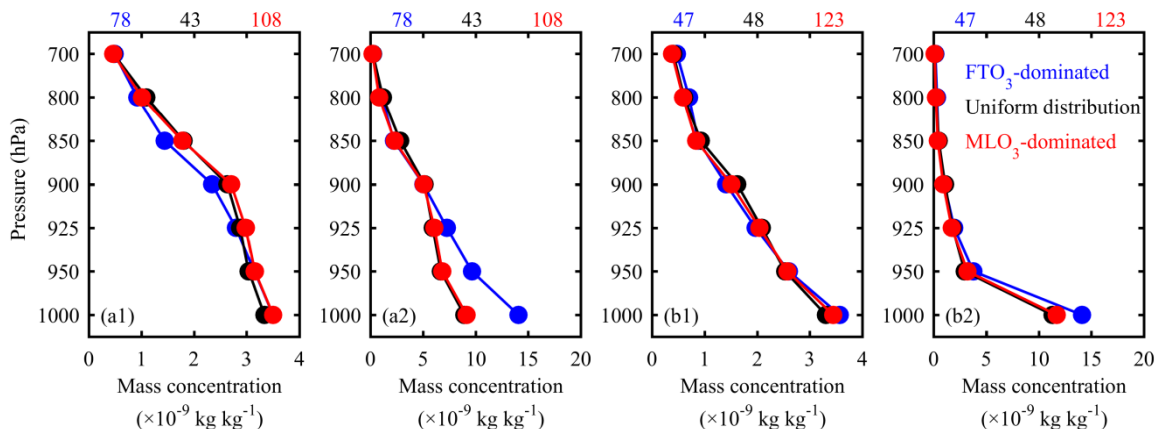


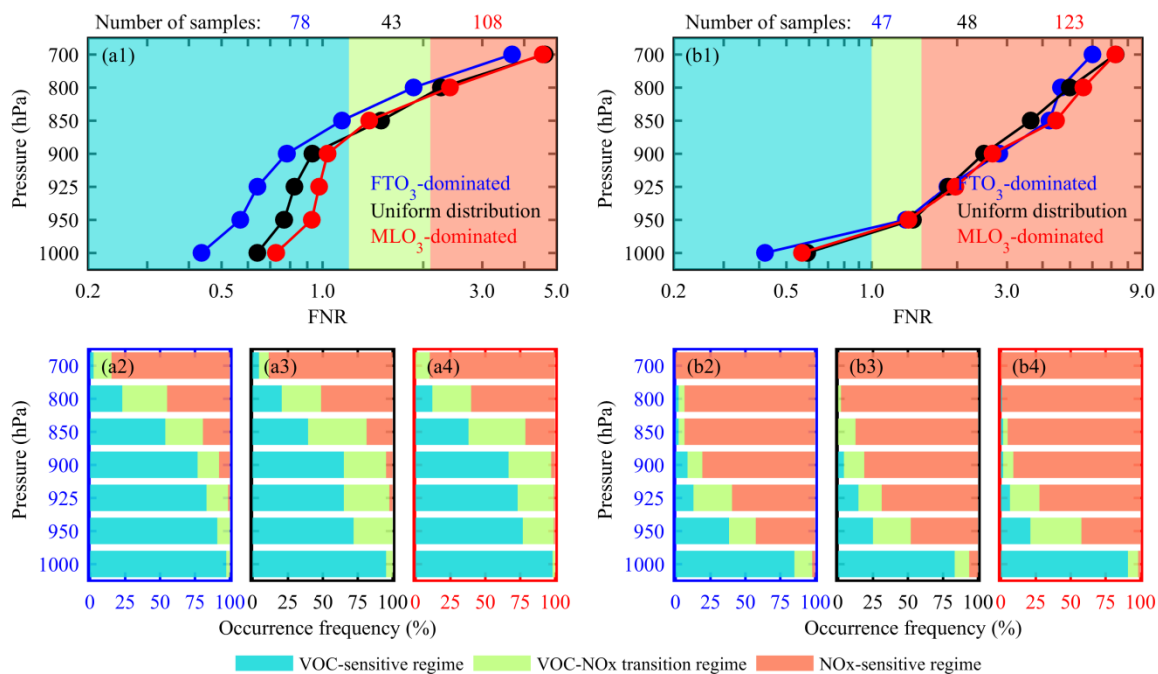
Figure 10. Composed vertical distributions (lower panel) of ozone precursors (1)  $\text{CH}_2\text{O}$  and (2)  $\text{NO}_2$  according to different ozone profile patterns in (a) summer of Beijing and (b) autumn of Hong Kong. The digits at the upper of plots denote the sample numbers in each of patterns.

Ozone production is nonlinearly dependent on the relative availability of  $\text{NO}_x$  versus VOCs. Owing to the nonlinear relationship between  $\text{O}_3$  and its precursors, net production of  $\text{O}_3$  is subject to both absolute concentrations of VOC and  $\text{NO}_x$  and their relative ratio, which determines the  $\text{O}_3$  production sensitivity. Based on the  $\text{CH}_2\text{O}/\text{NO}_2$  (FNR) photochemical indicator method, we further diagnosed  $\text{O}_3$  production sensitivity to its precursors among different  $\text{O}_3$  profile patterns (Fig. 11). In Beijing, the averaged FNR values in the ML (< 850 hPa) differ significantly among the different  $\text{O}_3$  profile patterns. From 900 to 700 hPa, the averaged FNR values increase quickly, causing a shift of  $\text{O}_3$  production sensitivity from VOC-limited to  $\text{NO}_x$ -limited. Daily statistics indicates that there is a significant increase of the transition regime frequency from  $\text{FTO}_3$ -dominated pattern to  $\text{MLO}_3$ -dominated pattern, whereas the occurrence of the VOC-limited regime shows an opposite trend. Vertically, the transition regime frequency increases with height in the ML (< 850 hPa), regardless of the  $\text{O}_3$  profile pattern. This is broadly similar to the MAX-DOAS-based findings of Chi et al. (2018), who reported that the transition regime accounted for 27.3% at 300 m height, but 50.0% at 1,100 m height over Beijing. In Hong Kong, the averaged FNR values increase more rapidly with height than in Beijing, but show small differences among the different  $\text{O}_3$  profile

patterns. The shift height of  $O_3$  production sensitivity in Hong Kong (approximately 950 hPa) is lower than that in Beijing. Daily statistics reveal that below this height,  $O_3$  production chemistry is overwhelmingly controlled by the VOC-limited regime, and above by the NOx-limited regime. Similar results had been reported via MAX-DOAS observations in Guangzhou (a megacity ~110 km northwest of Hong Kong), where  $O_3$  production sensitivity changed with height from VOC-limited (0.02–0.22 km) to transitional (0.22–0.42 km) to NOx-limited (0.42–2.02 km) (Lin et al., 2022).

485

Near the surface,  $O_3$  production chemistry is usually VOC-limited in both Beijing and Hong Kong. Controlled by VOC-limited regime,  $O_3$  production increases with increasing VOCs but decreases with NO<sub>x</sub> due to titration reaction ( $NO + O_3 \rightarrow NO_2$ ). From the FTO<sub>3</sub>-dominated to MLO<sub>3</sub>-dominated pattern, NO<sub>2</sub> concentration has a pronounced decrease in both megacities, suggesting a weakening of ozone consumption from NO titration. 490 Meanwhile, CH<sub>2</sub>O concentration has a more or less increase, suggesting increased potentiality of high-concentration  $O_3$  production. This potentiality can be easily realized on the MLO<sub>3</sub>-dominated days owing to the hot-dry weather conditions, particularly in Beijing. In the upper ML,  $O_3$  production chemistry in Beijing is dominated by VOC-limited and transition regimes. From the FTO<sub>3</sub>-dominated to MLO<sub>3</sub>-dominated pattern, there is a significant increase in CH<sub>2</sub>O concentration in the upper ML of Beijing. Therefore, higher-concentration  $O_3$  495 production can be expected in upper ML owing to more favorable sensitivity condition, in consistent with the observational result of sickle-shape  $O_3$  profile in the lower troposphere of Beijing. On the contrary,  $O_3$  production chemistry in the upper ML of Hong Kong is dominated by NO<sub>x</sub>-limited and transition regimes. From FTO<sub>3</sub>-dominated pattern to MLO<sub>3</sub>-dominated pattern, there is an insignificant change in NO<sub>2</sub> concentration in the upper ML of Hong Kong. This suggests that the high-concentration MLO<sub>3</sub> in Hong Kong cannot be well explained by 500 local photochemical production. Considering the higher wind speed associated with MLO<sub>3</sub>-dominated pattern in Hong Kong (Fig. 9), Regional transport may be an important factor influencing lower-tropospheric ozone distribution over Hong Kong.



505 Figure 11. Vertical characteristics of ozone production sensitivity according to different ozone profile patterns in (a) summer of Beijing and (b) autumn of Hong Kong. Upper panels (1) denote vertical FNR profiles. Lower panels (2),

3, and 4) denote the occurrence frequency of ozone production sensitivity in  $\text{FTO}_3$ -dominated, uniform distribution, and  $\text{MLO}_3$ -dominated patterns. The digits at the upper of plots denote the sample numbers in each of patterns.

## 510 4 Summary

We investigate lower tropospheric  $\text{O}_3$  distribution over two Chinese megacities (Beijing and Hong Kong) by introducing a novel mixing-layer-height-referenced ( $h$ -referenced)  $\text{O}_3$  climatology, in which lower tropospheric  $\text{O}_3$  profiles are scaled according to mixing layer top height  $h$ . Mixing layer top height was determined by an integral method that integrates temperature, humidity, and cloud profiles. We focused on the lower troposphere (below  $2 \times h$ ), with each profile subdivided in two compartments: the mixing layer and free troposphere (ML and FT). By examining  $\text{O}_3$  concentration differences between the ML and FT (i.e.,  $\text{MLO}_3$  and  $\text{FTO}_3$ ), all individual  $\text{O}_3$  profiles were classified into three typical patterns:  $\text{MLO}_3$ -dominated,  $\text{FTO}_3$ -dominated, and uniform distribution. Multi-scale meteorology and  $\text{O}_3$  precursors ( $\text{CH}_2\text{O}$  and  $\text{NO}_2$ ) were further analyzed to characterize the main physiochemical processes driving the different  $\text{O}_3$  profile patterns in polluted seasons (summer in Beijing and autumn in Hong Kong). Our conclusions are as follows:

- (1) Compared with traditional sea-level-referenced climatology,  $h$ -referenced  $\text{O}_3$  climatology preserves the dependence of  $\text{O}_3$  abundance and its variability on mixing layer top height, highlighting an inflection point (or discontinuity) at the interface between the ML and FT.
- (2) Mixing layer  $\text{O}_3$  concentrations show summer-high/winter-low climatology in Beijing, and autumn-high/summer-low climatology in Hong Kong. In the photochemical active season (summer in Beijing and autumn in Hong Kong), seasonal lower-tropospheric  $\text{O}_3$  profiles exhibit a sickle-shape pattern with a marked drop in concentrations from high values in the upper ML to low values in the lower FT. This sickle-shape profile pattern is significantly different from monotone increasing profile patterns across the rest of the year.
- (3) Highly variable  $\text{O}_3$  gradients in the lower troposphere, particularly at the surface layer and ML-FT interface, reflect the universality of vertical  $\text{O}_3$  stratification structure.  $\text{O}_3$  stratification in Hong Kong is stronger than that in Beijing. The stratification in the surface layer is likely due to strong titration chemical processes, and that at the ML-FT interface is attributable to the dynamic transport barrier of mixing layer capping inversion on vertical exchange. The contrasting  $\text{O}_3$  gradients at the ML-FT interface indicate different transport barrier effects, which typically shift from a ML-to-FT detrainment barrier in summer (autumn) to a FT-to-ML entrainment barrier in other seasons in Beijing (Hong Kong).
- (4)  $\text{FTO}_3$ -dominated pattern represents the most common  $\text{O}_3$  profile patterns in both Beijing and Hong Kong (occurrence frequencies of 69% and 54%, respectively). However,  $\text{MLO}_3$ -dominated pattern prevails in the photochemical active season, accounting for 46% of summer days in Beijing and 55% of autumn days in Hong Kong, which is more frequent than the previously reported episodic occurrence in northern mid-altitudes, indicating intensive  $\text{MLO}_3$  production in high-emission Chinese megacities. In polluted seasons (summer in Beijing and autumn in Hong Kong), the cross-pattern  $\text{O}_3$  profiles present a small difference in the FT part but a wide-range variability in the ML part, indicating that  $\text{MLO}_3$  production shapes the distinct  $\text{O}_3$  profile patterns.
- (5) From the  $\text{FTO}_3$ -dominated to  $\text{MLO}_3$ -dominated pattern, large-scale meteorology is characterized by increased geopotential height and downward ultraviolet radiation. Locally, there are no vertical structural differences in lower tropospheric meteorological profiles ( $\theta$ , RH, and WS) among the different  $\text{O}_3$  profile patterns. The maximum positive  $\theta$  gradient at the ML-FT interface demonstrates the common existence of mixing layer capping inversion, which acts as a barrier to vertical exchange. Low humidity represents a common factor associated with  $\text{MLO}_3$ -dominated pattern in both Beijing and Hong Kong.

(6) From the  $\text{FTO}_3$ -dominated to  $\text{MLO}_3$ -dominated pattern, the  $\text{O}_3$  precursor  $\text{CH}_2\text{O}$  ( $\text{NO}_2$ ) substantially increases (decrease) in Beijing, but increases (decreases) slightly in Hong Kong. In Beijing, the  $\text{CH}_2\text{O}$  increment is larger in the upper ML, whereas the  $\text{NO}_2$  decrement is larger in the lower ML. Such changes in  $\text{O}_3$  precursors push  $\text{O}_3$  production sensitivity away from the VOC-limited regime (towards higher  $\text{NO}_x$  sensitivity) and facilitate net production of  $\text{O}_3$  via photochemical reactions in the upper ML.

555

560

Comparing the above results with previous northern mid-latitude observations (Petetin et al., 2018), lower troposphere  $\text{O}_3$  variability over high-emission Chinese megacities is more likely controlled by  $\text{O}_3$ -related chemical processes, including titration consumption and photochemical production. From our comparison of Beijing and Hong Kong, lower troposphere  $\text{O}_3$  variability in China is not only subject to precursor emissions, but also reflects local topographical and meteorological characteristics. Therefore, to achieve comprehensive understanding of lower troposphere  $\text{O}_3$  variability in China, more ozonesonde observations over more sites are needed in the future.

### **Data availability**

565

Ozonesonde data for Beijing are available from the first author upon reasonable request ([lzhiheng118@163.com](mailto:lzhiheng118@163.com)).

Ozonesonde data for Hong Kong are available at <https://woudc.org/home.php?lang=en>.

ERA5-based meteorological reanalysis data are available at <https://cds.climate.copernicus.eu/>.

EAC4-based ozone precursor reanalysis data are available at <https://ads.atmosphere.copernicus.eu/>.

570

### **Author contributions**

ZL and SF designed the research. ZL organized and wrote the manuscript. MG and JQ edited the manuscript. JS contributed to satellite data analysis and code writing. JZ and YP contributed to ozonesonde observations in Beijing. All authors contributed to the revision of the manuscript.

575

### **Competing interests**

The contact author has declared that none of the authors has any competing interests.

### **Disclaimer**

580

Publisher's note: Copernicus Publications remains neutral with regard to jurisdictional claims in published maps and institutional affiliations.

### **Financial support**

585

This work is supported by the major project of Basic and Applied Basic Research project of Guangdong Province (grant no. 2020B0301030004), the Key-Area Research and Development Program of Guangdong Province (grant no. 2020B1111360003), the National Natural Science Foundation of China (grant no. 42293321 and 41975181).

### **References**

590

Benish, S. E., He, H., Ren, X. R., Roberts, S. J., Salawitch, R. J., Li, Z. Q., Wang, F., Wang, Y. Y., Zhang, F., Shao, M., Lu, S. H., and Dickerson, R. R.: Measurement report: Aircraft observations of ozone, nitrogen oxides, and volatile organic compounds over Hebei Province, China, *Atmos Chem Phys*, 20, 14523-14545, 10.5194/acp-20-14523-2020, 2020.

Berkes, F., Hoor, P., Bozem, H., Kunkel, D., Sprenger, M., and Henne, S.: Airborne observation of mixing across the entrainment zone during PARADE 2011, *Atmos. Chem. Phys.*, 16, 6011-6025, 10.5194/acp-16-6011-2016, 2016.

Chen, Z., Xie, Y., Liu, J., Shen, L., Cheng, X., Han, H., Yang, M., Shen, Y., Zhao, T., and Hu, J.: Distinct seasonality in vertical variations of tropospheric ozone over coastal regions of southern China, *Sci Total Environ*, 874, 162423,

595 <https://doi.org/10.1016/j.scitotenv.2023.162423>, 2023.

Chi, X. Y., Liu, C., Xie, Z. Q., Fan, G. Q., Wang, Y., He, P. Z., Fan, S. D., Hong, Q. Q., Wang, Z., Yu, X. W., Yue, F. E., Duan, J. B., Zhang, P. F., and Liu, J. G.: Observations of ozone vertical profiles and corresponding precursors in the low troposphere in Beijing, China, *Atmos Res*, 213, 224-235, 10.1016/j.atmosres.2018.06.012, 2018.

600 Diab, R. D., Thompson, A. M., Mari, K., Ramsay, L., and Coetzee, G. J. R.: Tropospheric ozone climatology over Irene, South Africa, from 1990 to 1994 and 1998 to 2002, *J Geophys Res-Atmos*, 109, Artn D20301 10.1029/2004jd004793, 2004.

Ding, A. J., Wang, T., Thouret, V., Cammas, J. P., and Nedelev, P.: Tropospheric ozone climatology over Beijing: analysis of aircraft data from the MOZAIC program, *Atmos Chem Phys*, 8, 1-13, Doi 10.5194/acp-8-1-2008, 2008.

605 Ding, A. J., Wang, T., and Fu, C. B.: Transport characteristics and origins of carbon monoxide and ozone in Hong Kong, South China, *J Geophys Res-Atmos*, 118, 9475-9488, 10.1002/jgrd.50714, 2013.

Donnell, E. A., Fish, D. J., Dicks, E. M., and Thorpe, A. J.: Mechanisms for pollutant transport between the boundary layer and the free troposphere, *Journal of Geophysical Research: Atmospheres*, 106, 7847-7856, <https://doi.org/10.1029/2000JD900730>, 2001.

610 Duncan, B. N., Yoshida, Y., Damon, M. R., Douglass, A. R., and Witte, J. C.: Temperature dependence of factors controlling isoprene emissions, *Geophysical Research Letters*, 36, <https://doi.org/10.1029/2008GL037090>, 2009.

Fleming, Z. L., Doherty, R. M., von Schneidemesser, E., Malley, C. S., Cooper, O. R., Pinto, J. P., Colette, A., Xu, X. B., Simpson, D., Schultz, M. G., Lefohn, A. S., Hamad, S., Moolla, R., Solberg, S., and Feng, Z. Z.: Tropospheric Ozone Assessment Report: Present-day ozone distribution and trends relevant to human health, *Elementa-Sci Anthrop*, 6, Artn 12 10.1525/Elementa.273, 2018.

615 Han, S., Yao, Q., Tie, X., Zhang, Y., Zhang, M., Li, P., and Cai, Z.: Analysis of surface and vertical measurements of O3 and its chemical production in the NCP region, China, *Atmos Environ*, 241, 117759, <https://doi.org/10.1016/j.atmosenv.2020.117759>, 2020.

He, G. W., Deng, T., Wu, D., Wu, C., Huang, X. F., Li, Z. N., Yin, C. Q., Zou, Y., Song, L., Ouyang, S. S., Tao, L. P., and Zhang, X.: Characteristics of boundary layer ozone and its effect on surface ozone concentration in Shenzhen, China: A case study, *Sci Total Environ*, 791, ARTN 148044 10.1016/j.scitotenv.2021.148044, 2021.

620 Hersbach, H., Bell, B., Berrisford, P., Hirahara, S., Horanyi, A., Munoz-Sabater, J., Nicolas, J., Peubey, C., Radu, R., Schepers, D., Simmons, A., Soci, C., Abdalla, S., Abellana, X., Balsamo, G., Bechtold, P., Biavati, G., Bidlot, J., Bonavita, M., De Chiara, G., Dahlgren, P., Dee, D., Diamantakis, M., Dragani, R., Flemming, J., Forbes, R., Fuentes, M., Geer, A., Haimberger, L., Healy, S., Hogan, R. J., Holm, E., Janiskova, M., Keeley, S., Laloyaux, P., Lopez, P., Lupu, C., Radnoti, G., de Rosnay, P., Rozum, I., Vamborg, F., Villaume, S., and Thepaut, J. N.: The ERA5 global reanalysis, *Q J Roy Meteor Soc*, 146, 1999-2049, 10.1002/qj.3803, 2020.

625 Inness, A., Ades, M., Agustí-Panareda, A., Barré, J., Benedictow, A., Blechschmidt, A. M., Dominguez, J. J., Engelen, R., Eskes, H., Flemming, J., Huijnen, V., Jones, L., Kipling, Z., Massart, S., Parrington, M., Peuch, V. H., Razinger, M., Remy, S., Schulz, M., and Suttie, M.: The CAMS reanalysis of atmospheric composition, *Atmos. Chem. Phys.*, 19, 3515-3556, 10.5194/acp-19-3515-2019, 2019.

Jaffe, D.: Relationship between Surface and Free Tropospheric Ozone in the Western U.S., *Environ Sci Technol*, 45, 432-438, 10.1021/es1028102, 2011.

630 Jin, X. M., Fiore, A., Boersma, K. F., De Smedt, I., and Valin, L.: Inferring Changes in Summertime Surface Ozone-NOx-VOC Chemistry over US Urban Areas from Two Decades of Satellite and Ground-Based Observations, *Environ Sci Technol*, 54, 6518-6529, 10.1021/acs.est.9b07785, 2020.

Kalabokas, P. D., Cammas, J. P., Thouret, V., Volz-Thomas, A., Boulanger, D., and Repapis, C. C.: Examination of the

atmospheric conditions associated with high and low summer ozone levels in the lower troposphere over the eastern  
640 Mediterranean, *Atmos Chem Phys*, 13, 10339-10352, 10.5194/acp-13-10339-2013, 2013.

Kalabokas, P. D., Thouret, V., Cammas, J. P., Volz-Thomas, A., Boulanger, D., and Repapis, C. C.: The geographical distribution of meteorological parameters associated with high and low summer ozone levels in the lower troposphere and the boundary layer over the eastern Mediterranean (Cairo case), *Tellus B*, 67, Artn 27853  
10.3402/Tellusb.V67.27853, 2015.

645 Karl, T., Lamprecht, C., Graus, M., Cede, A., Tiefengraber, M., Vila-Guerau de Arellano, J., Gurarie, D., and Lenschow, D.: High urban NO<sub>x</sub> triggers a substantial chemical downward flux of ozone, *Science Advances*, 9, eadd2365, 10.1126/sciadv.add2365, 2023.

Kaser, L., Patton, E. G., Pfister, G. G., Weinheimer, A. J., Montzka, D. D., Flocke, F., Thompson, A. M., Stauffer, R. M., and Halliday, H. S.: The effect of entrainment through atmospheric boundary layer growth on observed and modeled surface ozone in the Colorado Front Range, *J Geophys Res-Atmos*, 122, 6075-6093, 10.1002/2016JD026245, 2017.

650 Li, R. Y., Xu, M. Q., Li, M. C., Chen, Z. Y., Zhao, N., Gao, B. B., and Yao, Q.: Identifying the spatiotemporal variations in ozone formation regimes across China from 2005 to 2019 based on polynomial simulation and causality analysis, *Atmos Chem Phys*, 21, 15631-15646, 10.5194/acp-21-15631-2021, 2021.

Liao, Z., Ling, Z., Gao, M., Sun, J., Zhao, W., Ma, P., Quan, J., and Fan, S.: Tropospheric Ozone Variability Over Hong Kong Based on Recent 20 years (2000–2019) Ozonesonde Observation, *Journal of Geophysical Research: Atmospheres*, 126, e2020JD033054, <https://doi.org/10.1029/2020JD033054>, 2021.

655 Liao, Z. H., Pan, Y. B., Ma, P. K., Jia, X. C., Cheng, Z. G., Wang, Q. Q., Dou, Y. J., Zhao, X. J., Zhang, J. Q., and Quan, J. N.: Meteorological and chemical controls on surface ozone diurnal variability in Beijing: A clustering-based perspective, *Atmos Environ*, 295, ARTN 119566  
10.1016/j.atmosenv.2022.119566, 2023.

660 Lin, C. H., Wu, Y. L., and Lai, C. H.: Ozone reservoir layers in a coastal environment - a case study in southern Taiwan, *Atmos. Chem. Phys.*, 10, 4439-4452, 10.5194/acp-10-4439-2010, 2010.

Lin, H., Xing, C., Hong, Q., Liu, C., Ji, X., Liu, T., Lin, J., Lu, C., Tan, W., Li, Q., and Liu, H.: Diagnosis of Ozone Formation Sensitivities in Different Height Layers via MAX - DOAS Observations in Guangzhou, *Journal of Geophysical Research: Atmospheres*, 127, 10.1029/2022jd036803, 2022.

665 Liu, Z., Zha, F., Wang, Y., Yuan, B., Liu, B., and Tang, G.: Vertical evolution of the concentrations and sources of volatile organic compounds in the lower boundary layer in urban Beijing in summer, *Chemosphere*, 332, 138767, <https://doi.org/10.1016/j.chemosphere.2023.138767>, 2023.

Lu, X., Hong, J. Y., Zhang, L., Cooper, O. R., Schultz, M. G., Xu, X. B., Wang, T., Gao, M., Zhao, Y. H., and Zhang, Y. H.: Severe Surface Ozone Pollution in China: A Global Perspective, *Environ Sci Tech Let*, 5, 487-494, 10.1021/acs.estlett.8b00366, 2018.

670 Mills, G., Pleijel, H., Malley, C. S., Sinha, B., Cooper, O. R., Schultz, M. G., Neufeld, H. S., Simpson, D., Sharps, K., Feng, Z., Gerosa, G., Harmens, H., Kobayashi, K., Saxena, P., Paoletti, E., Sinha, V., and Xu, X. B.: Tropospheric Ozone Assessment Report: Present-day tropospheric ozone distribution and trends relevant to vegetation, *Elementa-Sci Anthrop*, 6, Artn 47  
10.1525/Elementa.302, 2018.

675 Monks, P. S., Archibald, A. T., Colette, A., Cooper, O., Coyle, M., Derwent, R., Fowler, D., Granier, C., Law, K. S., Mills, G. E., Stevenson, D. S., Tarasova, O., Thouret, V., von Schneidemesser, E., Sommariva, R., Wild, O., and Williams, M. L.: Tropospheric ozone and its precursors from the urban to the global scale from air quality to short-lived climate forcer, *Atmos Chem Phys*, 15, 8889-8973, 10.5194/acp-15-8889-2015, 2015.

Neuman, J. A., Trainer, M., Aikin, K. C., Angevine, W. M., Brioude, J., Brown, S. S., de Gouw, J. A., Dube, W. P., Flynn, J. H., Graus, M., Holloway, J. S., Lefer, B. L., Nedelev, P., Nowak, J. B., Parrish, D. D., Pollack, I. B., Roberts, J. M., Ryerson, T. B.,

Smit, H., Thouret, V., and Wagner, N. L.: Observations of ozone transport from the free troposphere to the Los Angeles basin, *Journal of Geophysical Research: Atmospheres*, 117, <https://doi.org/10.1029/2011JD016919>, 2012.

685 Ogino, S. Y., Fujiwara, M., Shiotani, M., Hasebe, F., Matsumoto, J., Hoang, T. H. T., and Nguyen, T. T. T.: Ozone variations over the northern subtropical region revealed by ozonesonde observations in Hanoi, *J Geophys Res-Atmos*, 118, 3245-3257, 10.1002/jgrd.50348, 2013.

690 Oltmans, S. J., Johnson, B. J., Harris, J. M., Thompson, A. M., Liu, H. Y., Chan, C. Y., Vomel, H., Fujimoto, T., Brackett, V. G., Chang, W. L., Chen, J. P., Kim, J. H., Chan, L. Y., and Chang, H. W.: Tropospheric ozone over the North Pacific from ozonesonde observations, *J Geophys Res-Atmos*, 109, Artn D15s01 10.1029/2003jd003466, 2004.

Petetin, H., Thouret, V., Fontaine, A., Sauvage, B., Athier, G., Blot, R., Boulanger, D., Cousin, J. M., and Nédélec, P.: Characterising tropospheric O<sub>3</sub> and CO around Frankfurt over the period 1994–2012 based on MOZAIC–AGOS aircraft measurements, *Atmos. Chem. Phys.*, 16, 15147-15163, 10.5194/acp-16-15147-2016, 2016.

695 Petetin, H., Sauvage, B., Smit, H. G. J., Gheusi, F., Lohou, F., Blot, R., Clark, H., Athier, G., Boulanger, D., Cousin, J. M., Nedelec, P., Neis, P., Rohs, S., and Thouret, V.: A climatological view of the vertical stratification of RH, O<sub>3</sub> and CO within the PBL and at the interface with free troposphere as seen by IAGOS aircraft and ozonesondes at northern mid-latitudes over 1994–2016, *Atmos. Chem. Phys.*, 18, 9561-9581, 10.5194/acp-18-9561-2018, 2018.

700 Seidel, D. J., Ao, C. O., and Li, K.: Estimating climatological planetary boundary layer heights from radiosonde observations: Comparison of methods and uncertainty analysis, *Journal of Geophysical Research: Atmospheres*, 115, <https://doi.org/10.1029/2009JD013680>, 2010.

Seinfeld, J. H., and Pandis, S. N.: *Atmospheric Chemistry and Physics from Air Pollution to Climate Change*, third ed. John, W., Sons, Inc., 2016.

705 Stauffer, R. M., Thompson, A. M., and Young, G. S.: Tropospheric ozonesonde profiles at long-term US monitoring sites: 1. A climatology based on self-organizing maps, *J Geophys Res-Atmos*, 121, 1320-1339, 10.1002/2015JD023641, 2016.

Stauffer, R. M., Thompson, A. M., Oltmans, S. J., and Johnson, B. J.: Tropospheric ozonesonde profiles at long-term US monitoring sites: 2. Links between Trinidad Head, CA, profile clusters and inland surface ozone measurements, *J Geophys Res-Atmos*, 122, 1261-1280, 10.1002/2016JD025254, 2017.

710 Stull, R. B.: *An Introduction to Boundary Layer Meteorology*; Kluwer Academic Publishers, Dordrecht, The Netherlands., 1988.

Tang, G. Q., Zhu, X. W., Xin, J. Y., Hu, B., Song, T., Sun, Y., Zhang, J. Q., Wang, L. L., Cheng, M. T., Chao, N., Kong, L. B., Li, X., and Wang, Y. S.: Modelling study of boundary-layer ozone over northern China - Part I: Ozone budget in summer, *Atmos Res*, 187, 128-137, 10.1016/j.atmosres.2016.10.017, 2017.

715 Trousdale, J. F., Conley, S. A., Post, A., and Faloona, I. C.: Observing entrainment mixing, photochemical ozone production, and regional methane emissions by aircraft using a simple mixed-layer framework, *Atmos. Chem. Phys.*, 16, 15433-15450, 10.5194/acp-16-15433-2016, 2016.

Wang, P., Yang, Y., Li, H., Chen, L., Dang, R., Xue, D., Li, B., Tang, J., Leung, L. R., and Liao, H.: North China Plain as a hot spot of ozone pollution exacerbated by extreme high temperatures, *Atmos. Chem. Phys.*, 22, 4705-4719, 10.5194/acp-22-4705-2022, 2022a.

720 Wang, T., Xue, L., Brimblecombe, P., Lam, Y. F., Li, L., and Zhang, L.: Ozone pollution in China: A review of concentrations, meteorological influences, chemical precursors, and effects, *Sci Total Environ*, 575, 1582-1596, <https://doi.org/10.1016/j.scitotenv.2016.10.081>, 2017.

Wang, T., Xue, L., Feng, Z., Dai, J., Zhang, Y., and Tan, Y.: Ground-level ozone pollution in China: a synthesis of recent findings on influencing factors and impacts, *Environmental Research Letters*, 17, 063003, 10.1088/1748-9326/ac69fe, 725 2022b.

Wang, X. Y., and Wang, K. C.: Estimation of atmospheric mixing layer height from radiosonde data, *Atmos. Meas. Tech.*, 7,

1701-1709, 10.5194/amt-7-1701-2014, 2014.

Williams, A. G., Zahorowski, W., Chambers, S., Griffiths, A., Hacker, J. M., Element, A., and Werczynski, S.: The Vertical Distribution of Radon in Clear and Cloudy Daytime Terrestrial Boundary Layers, *Journal of the Atmospheric Sciences*, 68, 155-174, <https://doi.org/10.1175/2010JAS3576.1>, 2011.

730 Wyngaard, J. C., and Brost, R. A.: Top-Down and Bottom-Up Diffusion of a Scalar in the Convective Boundary Layer, *Journal of Atmospheric Sciences*, 41, 102-112, [https://doi.org/10.1175/1520-0469\(1984\)041<0102:TDABUD>2.0.CO;2](https://doi.org/10.1175/1520-0469(1984)041<0102:TDABUD>2.0.CO;2), 1984.

Xu, Z., Chen, H., Guo, J., and Zhang, W.: Contrasting Effect of Soil Moisture on the Daytime Boundary Layer Under Different Thermodynamic Conditions in Summer Over China, *Geophysical Research Letters*, 48, e2020GL090989, <https://doi.org/10.1029/2020GL090989>, 2021.

735 Yates, E. L., Johnson, M. S., Iraci, L. T., Ryoo, J. M., Pierce, R. B., Cullis, P. D., Gore, W., Ives, M. A., Johnson, B. J., Leblanc, T., Marrero, J. E., Sterling, C. W., and Tanaka, T.: An Assessment of Ground Level and Free Tropospheric Ozone Over California and Nevada, *Journal of Geophysical Research: Atmospheres*, 122, 10,089-010,102, <https://doi.org/10.1002/2016JD026266>, 2017.

740 Yonemura, S., Tsuruta, H., Kawashima, S., Sudo, S., Peng, L. C., Fook, L. S., Johar, Z., and Hayashi, M.: Tropospheric ozone climatology over Peninsular Malaysia from 1992 to 1999, *Journal of Geophysical Research: Atmospheres*, 107, ACH 1-1-ACH 1-12, <https://doi.org/10.1029/2001JD000993>, 2002.

Yu, S. C.: Fog geoengineering to abate local ozone pollution at ground level by enhancing air moisture, *Environ Chem Lett*, 17, 565-580, 10.1007/s10311-018-0809-5, 2019.

745 Zhang, J., Li, D., Bian, J., Xuan, Y., Chen, H., Bai, Z., Wan, X., Zheng, X., Xia, X., and Lü, D.: Long-term ozone variability in the vertical structure and integrated column over the North China Plain: results based on ozonesonde and Dobson measurements during 2001–2019, *Environmental Research Letters*, 16, 074053, 10.1088/1748-9326/ac109f, 2021.

Zhao, W., Tang, G. Q., Yu, H., Yang, Y., Wang, Y. H., Wang, L. L., An, J. L., Gao, W. K., Hu, B., Cheng, M. T., An, X. Q., Li, X., and Wang, Y. S.: Evolution of boundary layer ozone in Shijiazhuang, a suburban site on the North China Plain, *J Environ Sci*, 83, 152-160, 10.1016/j.jes.2019.02.016, 2019.

Zhu, X. W., Ma, Z. Q., Qiu, Y. L., Liu, H., Liu, Q., and Yin, X. M.: An evaluation of the interaction of morning residual layer ozone and mixing layer ozone in rural areas of the North China Plain, *Atmos Res*, 236, ARTN 104788 10.1016/j.atmosres.2019.104788, 2020.

755